Structural basis for regulation of Frizzled-4 signaling by the co-receptor Tetraspanin-12

Alyana J. Granados[1,3], Payal P. Pratap[1,3], Kevin Alexander Estrada Alamo[1,2], Katherine J. Susa[1,†]

[1] Department of Pharmaceutical Chemistry, University of California, San Francisco, CA 94158, USA

[2] Program in Biophysics, University of California, San Francisco, CA 94158, USA

[3] These authors contributed equally.

[†]Correspondence and requests for materials should be sent to Katherine J. Susa (Katherine.Susa@ucsf.edu)

ABSTRACT

Norrin is an atypical ligand that regulates retinal angiogenesis through the Wnt/β-catenin pathway by triggering heterodimerization of Frizzled-4 (FZD4) with Low-density lipoprotein receptor-related protein 5 or 6 (LRP5/6), leading to downstream β-catenin stabilization. Unlike Wnt ligands, Norrin requires the tetraspanin Tspan12 for signaling amplification, but it is not understood why. Here, we report a 3.4-angstrom structure of Tspan12 in complex with FZD4 determined by cryo-electron microscopy. The structure reveals that FZD4 and Tspan12 form a direct complex in the absence of Norrin, with a contact interface between the lower hinge of FZD4 and the extracellular loops of Tspan12 that enables FZD4 to respond with a more gradual response to a wider range of Norrin concentrations. The transmembrane (TM) domain of Tspan12 is oriented in a tightly packed four-helix bundle and interacts with TM2 of FZD4 to promote trafficking of Tspan12 to the cell surface. The C-D helices of Tspan12, which mediate binding to Norrin, remain exposed while Tspan12 is in complex with FZD4, facilitating higher-affinity Norrin binding. Cell-based assays reveal that Tspan12 and FZD4 remain associated after Norrin recognition, indicating that Tspan12 is a core component of the FZD4-Norrin-LRP5/6 signaling complex. Together, these studies reveal the molecular mechanism underlying Tspan12-FZD4 complex assembly and enhancement of Norrin signaling and suggest new ways to target the FZD4-Tspan12 complex for ocular diseases of hypo- or hyper-vascularization.

INTRODUCTION

Wnt/β-catenin signaling is a highly conserved cellular communication pathway that is one of the main regulators of development, cell fate determination, tissue homeostasis, and tissue regeneration in metazoans[1,2]. Wnts, a family of secreted, lipid-modified growth factors, initiate signaling by binding to G-protein coupled receptors (GPCRs) of the Frizzled family, which are characterized by an extracellular N-terminal cysteine-rich domain (CRD)[3,4]. Wnt binding within the CRD[5,6] promotes heterodimer formation with the co-receptor Low-density lipoprotein receptor-related protein 5 or 6 (LRP5/6)[7]. FZD-LRP5/6 heterodimers recruit the intracellular signaling effectors Dishevelled (Dvl)[8] and Axin[9], ultimately leading to stabilization of the transcriptional co-activator β-catenin and induction of Wnt target genes to drive cell division, migration, and differentiation[10]. In line with this, dysregulated signaling can lead to developmental defects, cancer, and degenerative disorders[1,2]

In the early 1990s, an atypical ligand that activates β-catenin signaling, Norrin (Norrie Disease Protein, NDP), was discovered through experiments aimed at identifying genes associated with Norrie disease, a neurodevelopmental disorder characterized by severe vision loss or blindness, intellectual disability, and hearing loss[11,12]. Norrin has a transforming growth factor-β-like cysteine knot fold and is homodimeric, consisting of two disulfide-linked protomers[13]. Norrin has no structural homology to Wnts yet mimics their function. Each Norrin protomer contains non-overlapping binding sites for the CRD of FZD4 and for LRP5/6, which triggers heterodimerization of FZD with LRP5/6 to initiate β-catenin signaling[14]. Unlike Wnt ligands, which bind promiscuously to multiple FZD family members[15], Norrin specifically binds to FZD4 out of the ten human Frizzled receptors[16]. Norrin/FZD4 signaling is essential for retinal blood vessel formation and blood-retina barrier development[17]. Consistent with this critical role, mutations in genes encoding components of this pathway—including Norrin, FZD4, and LRP5—cause familial exudative vitreoretinopathy (FEVR), a hereditary ocular disorder related to Norrie disease characterized by retinal hypo-vascularization, leading to retinal detachment, vision loss, or

blindness[18,19]. Additionally, Norrin plays important roles in angiogenesis for not only eye development but also in the ear, brain, and female reproductive system[13].

Compared to Wnt ligands, Norrin has the unique feature of utilizing a member of the tetraspanin family as a co-receptor to amplify β-catenin signaling. Nearly two decades after the identification of Norrin, a large-scale reverse genetic screen revealed that mutations in the gene encoding for Tetraspanin-12 (Tspan12) mimic the retinal vascular defects of NDP, FZD4, and LRP5 mutant mice[20].Tspan12 is a member of the ancient, highly conserved tetraspanin family of four-pass transmembrane proteins, which have been termed "molecular facilitators"[21]. Tetraspanins bind transmembrane partner proteins to regulate a range of fundamental signal transduction pathways[22,23], including B cell[24,25], Notch[26], and integrin[27,28] signaling through regulation of partner protein trafficking and membrane microdomain localization. Cell-based assays demonstrated that Tspan12 functions as a co-receptor to significantly increase Norrin/β-catenin signaling by about 4-fold, while having no effect on Wnt/β-catenin signaling[20]. In line with Tspan12's important role in amplifying Norrin signaling, mutations in Tspan12 cause FEVR and account for approximately 5-10% of FEVR cases in humans[18,19,29–33].

The mechanism underlying Tspan12 enhancement of FZD4 signaling has remained unclear, with proposed models including allosteric modulation of FZD4 to amplify signaling[34], promotion of FZD4 clustering[35], or enhancement of FZD4/LRP5 heterodimerization[36]. Tspan12 can rescue β-catenin signaling disrupted by point mutations that impair the Norrin-FZD4 interaction, indicating that Tspan12 may enhance the binding of Norrin to FZD4[34]. However, it is unclear whether Tspan12 achieves this function through a direct interaction with FZD4. Recent biophysical experiments showed that Tspan12 directly binds Norrin with high affinity (10 nM), and can bind the same protomer of Norrin as the CRD of FZD4[37]. However, Tspan12 is competitive for the same binding site on Norrin as LRP6[37]. These data support a ligand hand-off mechanism, in which Tspan12 initially promotes the capture of Norrin and then passes it off to FZD4 and LRP5/6[37]. An alternative mechanism is Tspan12 remaining incorporated in the Norrin-FZD4-

LRP5/6 complex, with Tspan12 and LRP5/6 each binding to separate protomers of Norrin. However, the structural basis for Tspan12 engaging a single protomer remains unclear.

To understand how Tspan12 mediates enhancement of Norrin signaling, we determined the structure of Tspan12 bound to FZD4 using single-particle cryo-electron microscopy (cryo-EM). We then used cell-based signaling assays to characterize how Norrin binds to the Tspan12-FZD4 complex and monitor Tspan12-FZD4 dynamics upon Norrin recognition. Our structural analysis and cell-based assays define the molecular basis for Tspan12 enhancement of Norrin signaling and suggest a model in which Tspan12 does not "hand off" Norrin to FZD4 and LRP5 but instead remains associated as a constitutive component of the FZD4-LRP5/6 signaling complex.

RESULTS

Engineering and structure determination of the Tspan12-FZD4 complex

Tspan12 requires interaction with FZD4 for trafficking to the cell surface[34] and co-localizes with FZD4 on the cell surface[13,34,35], suggesting a direct interaction that initiates in the endoplasmic reticulum[34]. However, our initial attempts to purify a stable Tspan12-FZD4 complex through co-expression and dual-affinity tag purification were unsuccessful, likely due to weak affinity between Tspan12-FZD4, which is consistent with prior reports for both Tspan12-FZD4 and other tetraspanin-partner complexes[37,38]. To overcome this, we engineered a construct with Tspan12 tethered to FZD4 to increase their local concentration and apparent affinity. This construct contains the full-length FZD4 sequence connected to full-length Tspan12 with a flexible glycine-glycine-serine (GGS) linker **(Supplementary Figure 1A)**.

To validate that this tethered construct maintains the natural interaction that facilitates FZD4-mediated trafficking of Tspan12 to the cell surface, we used a flow cytometry-based trafficking assay to monitor Tspan12 surface expression with an anti-Tspan12 antibody **(Figure 1A)**. While Tspan12 expressed alone showed low levels on the cell surface, co-expression with FZD4 resulted in a 4-fold increase in Tspan12 trafficking to the cell surface **(Figure 1A)**. The

tethered Tspan12-FZD4 construct displayed a similar magnitude of increase in Tspan12 surface trafficking as Tspan12 co-transfected with FZD4, indicating that our engineered construct retains the interaction that mediates Tspan12 trafficking and is properly folded **(Figure 1A)**.

Initial structure determination efforts for the Tspan12-FZD4 complex by single particle cryo-EM were unsuccessful due to the relatively small size of the complex (93 kDa) and limited rigid extracellular features outside of the detergent micelle. To overcome this, we introduced the thermostabilized BRIL domain (cytochrome b652 RIL) into intracellular loop 3 (ICL3) of FZD4, following previously reported successful structure determination of inactive state GPCRs that used an anti-BRIL Fab (BAG2) as a rigid fiducial marker to improve particle alignments[39,40]. To optimize a rigid connection between FZD4 and BRIL, we used AlphaFold3 to guide linker selection, choosing a linker that was predicted to form a continuous rigid helix with high confidence **(Supplementary Figure 1B-D)**[41]. We confirmed that the tethered FZD4-BRIL-Tspan12 construct maintained the ability to traffic Tspan12 to the cell surface. Our BRIL-engineered construct resulted in enhanced levels of Tspan12 and FZD4 on the cell surface **(Supplementary Figure 1E, F)**, indicating that the BRIL domain likely stabilizes FZD4 to result in higher expression levels, which is consistent with prior reports[42].

For structure determination, we incubated purified FZD4-BRIL-Tspan12 with anti-BRIL Fab[43] and an anti-Fab nanobody[44] **(Supplementary Figure 1G, H)**. Cryo-EM imaging of this complex revealed well-dispersed particles, and two-dimensional class averages showed clear secondary structures in both the Fab region and transmembrane region **(Supplementary Figure 2)**. Subsequent 3D refinement resulted in a structure of FZD4-BRIL-Tspan12 bound to the anti-BRIL F_{ab} and anti-F_{ab} nanobody at an overall nominal resolution of 3.4 Å, with density well defined for all features of the complex, except the N-terminal CRD-Hinge region of FZD4 and the C-terminal tail of Tspan12, both of which are highly flexible **(Figure 1B, Supplementary Table 1)**.

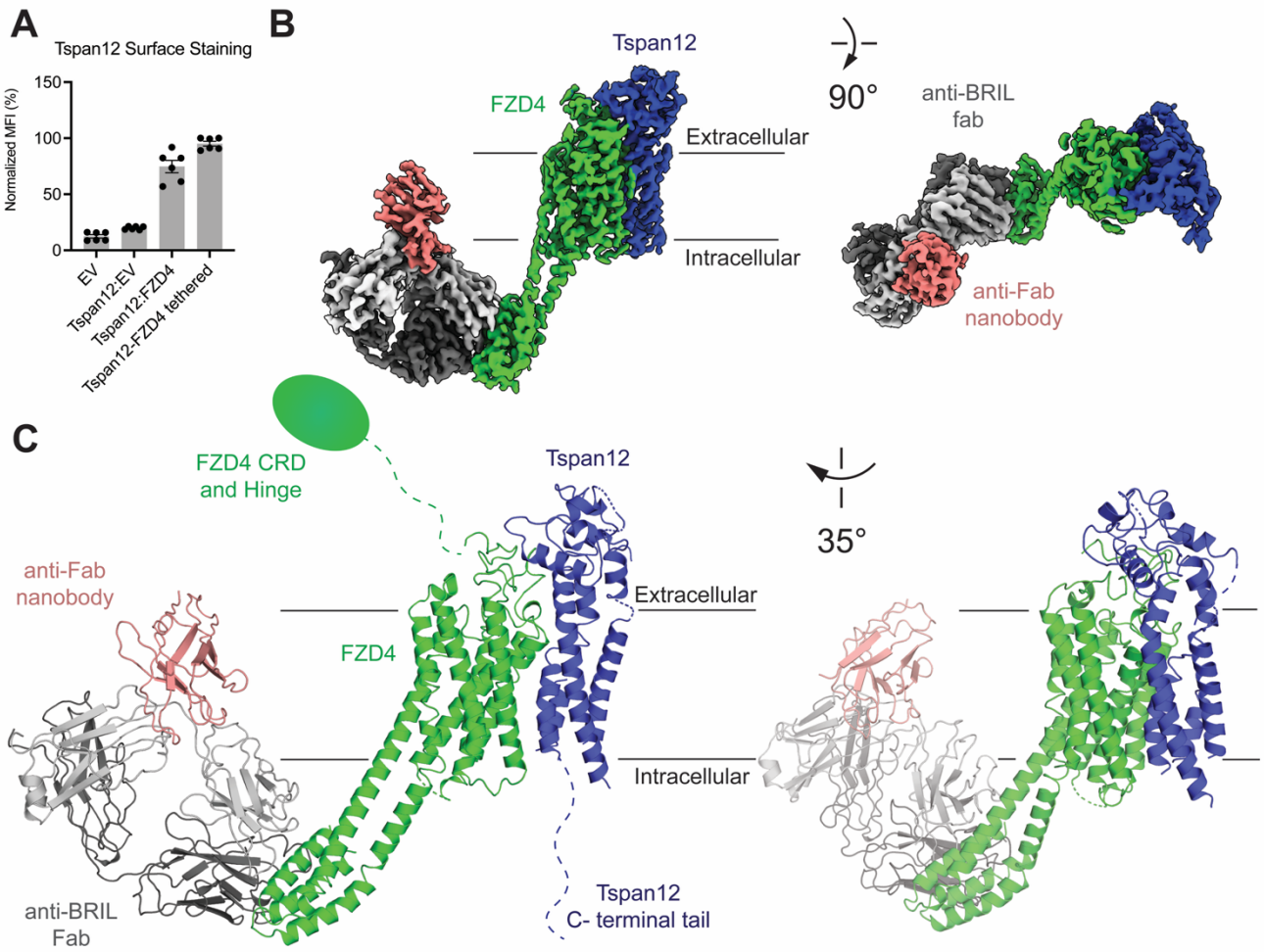

Figure 1: 3D reconstruction and atomic model of the human FZD4-Tspan12 complex bound to an anti-BRIL F_{ab} and anti-F_{ab} nanobody (PDB: 9YEV). (A) Tspan12 trafficking assay with either Tspan12 transfected with empty vector (EV), FZD4, or as a tethered complex with FZD4. Surface Tspan12 was detected by flow cytometry using an Alexa 647-coupled anti-Tspan12 antibody (Biotechne FAB8910R-025). **(B)** Different views of the cryo-EM map of the FZD4-Tspan12-anti-BRIL F_{ab}-anti-F_{ab} nanobody complex, colored by subunit. **(C)** Ribbon representation of the structure of the complex. FZD4, Tspan12, the anti-F_{ab} nanobody, and the anti-BRIL F_{ab} are colored as in B.

Tspan12 does not alter FZD4 conformation

To build the initial model, AlphaFold3[45] models of FZD4-BRIL and Tspan12, and the structure of the anti-BRIL-F_{ab} and anti-F_{ab} nanobody[39] were docked into the cryo-EM density map and manually rebuilt. While the FZD4 model fit readily into the density map, the transmembrane

helices of Tspan12 had to be separately docked due to differences in their orientation compared to the AlphaFold3 model **(Supplementary Figure 3)**. In the complex, Tspan12 packs against the second and third transmembrane domains (TM2 and TM3) of FZD4 via hydrophobic interactions and, interestingly, also makes contacts with extracellular loop 1 (ECL1) and the lower region of the hinge domain (also termed "linker") of FZD4, which is a flexible region connecting the CRD to the 7-transmembrane domain[40,46] **(Figure 1C, Supplementary Figure 3B-D)**. The FZD4-Tspan12 complex buries a total of approximately 1338 $Å^2$ at the interface between the ectodomains and transmembrane domains.

One model of Tspan12 enhancement of signaling is that Tspan12 allosterically activates FZD4 to enhance binding of the intracellular signaling effector Dvl[34]. However, recent experiments have shown that the affinity of the Dvl2 DEP domain for the Tspan12-FZD4 complex is not significantly different than its affinity for Fzd4 alone[37]. In line with this, the FZD4-Tspan12 structure shows no change in FZD4 conformation compared to the inactive state crystal structure of FZD4 (PDB: 6BD4), with a root mean square deviation (RMSD) of 0.68 Å **(Supplementary Figure 4A)**, indicating that Tspan12 is not functioning to allosterically activate FZD4[47]. A structure of FZD4 bound to the DEP domain of Dvl2 was also determined by cryo-EM (PDB: 8WMA), which revealed that DEP induces a subtle outward movement of TM6 (4.0 Å) and a slight inward movement of TM5 of FZD4[48]. Tspan12 binds to TM2 and TM3 of FZD4 and makes no contacts with FZD4 that would interfere with DEP engagement, indicating that it is possible for Tspan12 to remain bound to FZD4 after Dvl engagement **(Supplementary Figure 4B)**. While it is possible that the BRIL fusion may influence these structural comparisons, our results indicate that it is unlikely that Tspan12 plays a major allosteric role.

The C-D helices of Tspan12 are exposed within the FZD4 complex to facilitate higher affinity Norrin binding

Tspan12 is the only known tetraspanin identified to date with an obvious receptor function for an endogenous secreted ligand, binding to Norrin within its ectodomain with an affinity of 10 nM[34,37,49]. In line with this, Tspan12 has a particularly unique mode of engagement with FZD4 compared to other tetraspanin-partner structures **(Figure 2A and 2B)**. In addition to their four-pass transmembrane domain, tetraspanins have two extracellular domains, a small extracellular loop (SEL) and a large extracellular loop (LEL)[23]. Within the LEL, tetraspanins have two hypervariable helices, the "C" and "D" helices. Among different members of the tetraspanin family, these helices are highly variable in sequence and structure, and represent an important site in which structural variability in tetraspanins encodes specificity for their interactions with partners[23]. Two other structures of tetraspanins with non-tetraspanin partners have been reported to date at a resolution sufficient to build an atomic model—the tetraspanin CD81 with the B cell co-receptor CD19, and Tspan15 with the metalloprotease ADAM10[38,50]. In both these structures, the C and D helices create the main interaction interface with the partner protein. However, in the structure of Tspan12 bound to FZD4, the C and D helices are completely exposed and highly dynamic, making up the area of poorest local resolution in the cryo-EM map **(Supplementary Figure 5).** The C and D helices were recently shown to be the site of Norrin binding to Tspan12 using a high-confidence AlphaFold-Multimer prediction and model-guided point mutagenesis[37]. We used a flow-cytometry-based binding assay to measure the EC_{50} of Norrin binding to the FZD4-Tspan12 tethered construct with an E170K mutation in Helix D of Tspan12, which is predicted by the Norrin-Tspan12 AlphaFold model to form a hydrogen bond with Serine 83 of Norrin[37]. This construct bound Norrin with a 4-fold decrease in apparent affinity, confirming the C and D helices of Tspan12 mediate binding to Norrin while in the context of the FZD4-Tspan12 complex **(Figure 2C)**.

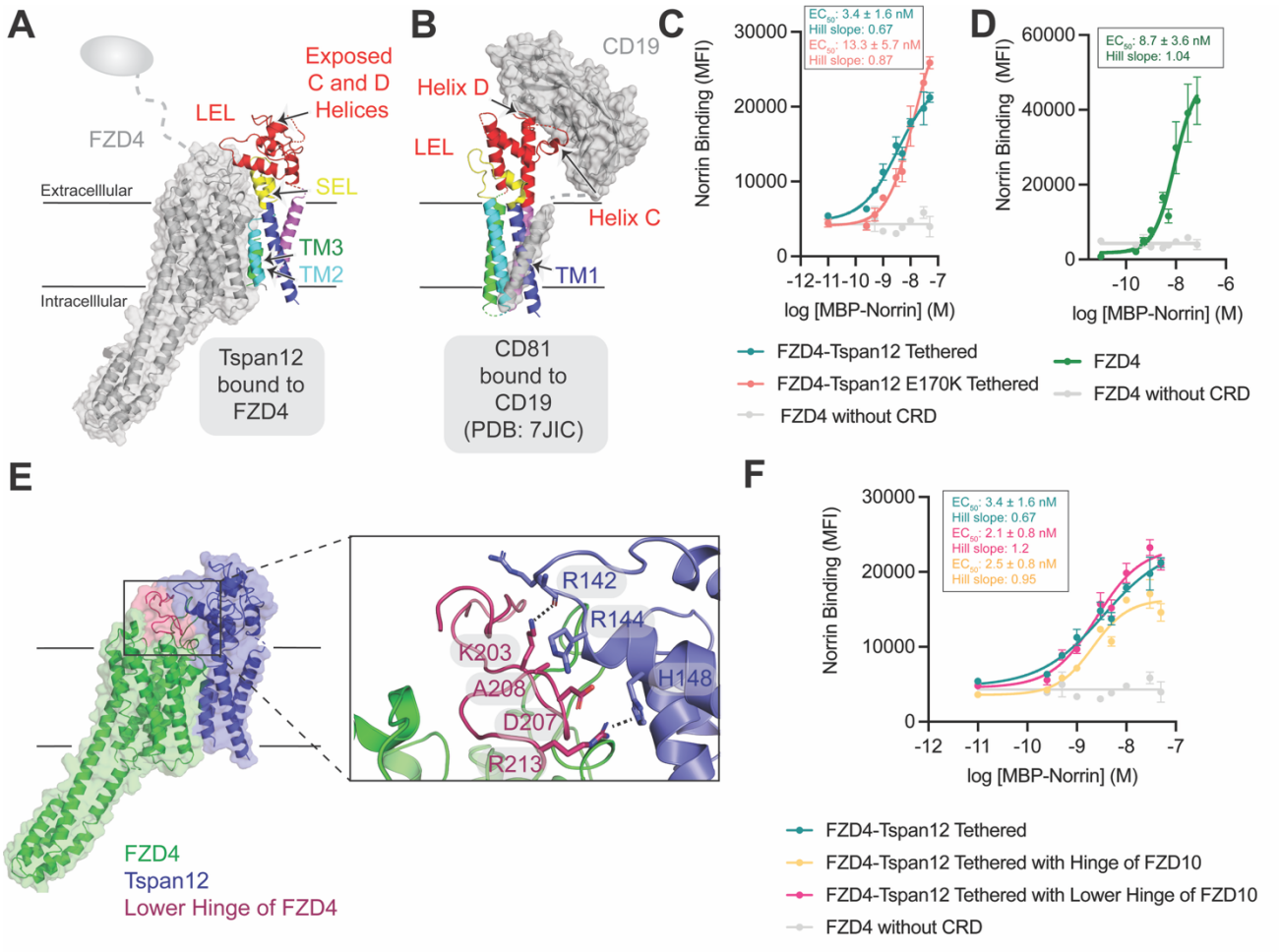

Figure 2: Characterization of Norrin binding to the FZD4-Tspan12 complex. (A and B) Comparison of the FZD4-Tspan12 complex to the CD19-CD81 complex (PDB: 7JIC). The partner protein is colored in grey, and the tetraspanin is colored by domain. The tetraspanin CD81 uses the C-D helices within the LEL as the primary engagement site with its partner CD19, while in the structure of FZD4-Tspan12, these two helices make no contact with the partner. **(C)** Binding of Norrin to Expi293 cells expressing either tethered FZD4-Tspan12 or tethered FZD4-Tspan12 with an E170K point mutation in the D helix Tspan12. Tethered FZD4-Tspan12: EC50: 3.4 ± 1.6 nM, Hill slope: 0.67. Tethered FZD4-Tspan12 E170K: EC50: 13.3 ± 5.7 nM, Hill slope: 0.87. **(D)** Binding of Norrin to Expi93 cells expressing apo-FZD4. EC50**:** 8.7 ± 3.6 nM, Hill slope: 1.04. **(E)** Interaction between the lower hinge of FZD4 and Tspan12, showing a zoomed-in interface. **(F)** Binding of Norrin to FZD4-Tspan12 hinge chimeras. Tethered FZD4-Tspan12: EC50: 3.4 ± 1.6 nM, Hill slope: 0.67. Tethered FZD4-Tspan12 with hinge of FZD10: EC50: 2.1 ± 0.8 nM, Hill slope: 1.2. Tethered FZD4-Tspan12 with lower hinge of FZD10: EC50: 2.5 ± 0.8 nM, Hill slope: 0.95. For all binding curves, experiments were performed in triplicate with error bars representing mean ± SEM. In all binding experiments, FZD4 without the CRD was used as a control for background binding.

Tspan12 modulates how FZD4 responds to Norrin

Tspan12 and FZD4 bind to non-overlapping regions on the same protomer of Norrin[37]. Because the C and D helices of Tspan12 remain accessible for Norrin capture when Tspan12 is bound to FZD4, we hypothesized that this may provide avidity to promote increased Norrin capture by positioning the CRD (the Norrin binding domain of FZD4) and the C-D helices of Tspan12 in close proximity. To test this, we measured the EC_{50} of Norrin binding to the tethered FZD4-Tspan12 construct compared to FZD4 alone using a flow cytometry-based binding assay. The tethered construct bound Norrin with approximately 2-fold higher apparent affinity, with an EC_{50} of 3.4 ± 1.6 nM for the FZD4-Tspan12 complex and 8.7 ± 3.6 nM for apo-FZD4 **(Figure 2C and 2D)**. Interestingly, the Hill slopes, a report on the cooperativity of binding, were also different between apo-FZD4 and FZD4 bound to Tspan12, indicating divergent degrees of cooperativity. The apo-FZD4 binding curve had a Hill slope of 1.0, while the Tspan12-FZD4 binding curve had a Hill slope of 0.67, consistent with a previous report that Tspan12 and FZD4 bind to Norrin with negative cooperativity[37]. While Norrin binds to apo-FZD4 with a sharper, switch-like response, Tspan12-FZD4 binds Norrin with a more gradual response, enabling binding over a wider concentration range of ligand. One mechanism to explain these results is that Tspan12 introduces steric constraints or orientation changes that make the binding of a second FZD4-Tspan12 complex to bind to the other protomer of Norrin less favorable. These data indicate that Tspan12 functions to modulate how FZD4 binds to Norrin to fine-tune signaling to enable a more graded response to a wider range of Norrin concentrations.

The Tspan12-FZD4 structure revealed that the LEL of Tspan12 interacts with the lower region of the hinge domain of FZD4 **(Figure 2E, Supplementary Figure 3B-C**). The hinge domain connects the CRD to the 7-TM domain of FZD receptors. This domain is highly variable in length and sequence among FZD family members and can be subdivided into a highly flexible segment from the CRD to the first conserved cysteine residue, followed by a shorter, more ordered segment from the first conserved cysteine to TM1[40]. While the CRD and upper hinge segment are

not observed in our structure due to inherent flexibility, a portion of the lower, ordered hinge segment makes several contacts with the LEL of Tspan12. Within the hinge, Lysine 203 of FZD4 hydrogen bonds with the carbonyl of Arginine 142 of Tspan12, and Arginine 213 of FZD4 interacts with Histidine 148 of Tspan12 **(Figure 2E, Supplementary Figure 3B-3C)**.

The hinge domain of FZD4 is essential for Norrin signaling. Swapping the FZD4 hinge with the FZD5 hinge results in a loss of Norrin signaling and a decrease in affinity for Norrin[51]. We next asked if Tspan12's interaction with the lower hinge of FZD4 contributes to the observed negative cooperativity in binding. To test this, we created FZD4-Tspan12 chimeras in which either the entire hinge domain or the lower hinge of FZD4 was replaced with that of FZD10 and measured the EC_{50} of these chimeras for Norrin. Both hinge chimeras bound to Norrin with approximately the same apparent affinity as the wild-type FZD4-Tspan12 tethered complex **(Figure 2F)**. However, the hill slope of both binding curves for the hinge chimeras was restored to approximately 1.0 **(Figure 2F)**, indicating that this region is an important contributor to how FZD4 recognizes Norrin and the observed negative cooperativity. Tspan12's interaction with the lower linker likely restrains the structural dynamics of this region, making it less likely for another FZD4 molecule to bind the second protomer of Norrin.

Interactions within the transmembrane domain mediate Tspan12 trafficking to the cell surface

Tspan12 and FZD4 initiate their partnership in the secretory pathway, and Tspan12 is dependent on FZD4 for proper trafficking to the cell surface[34]. This is highly unusual for a member of the tetraspanin family—in other tetraspanin-partner trafficking relationships studied to date, the tetraspanin is responsible for promoting the trafficking of the partner to the cell surface[52]. For example, the tetraspanin CD81 promotes the trafficking of its partner, CD19, to the cell surface by covering up an exposed, highly hydrophobic patch within the CD19 ectodomain, promoting the surface expression of properly folded CD19, and CD19 has no reciprocal effect on CD81 expression[38,53].

Next, we asked how FZD4 promotes trafficking of Tspan12 to the cell surface. We created a panel of FZD4 chimeras with domain swaps in domains that interact with Tspan12 **(Figure 3A, Supplementary Table 2, Supplementary Figure 6)**. We replaced either ECL1, TM2, TM3, or the lower hinge of FZD4 with that of FZD10 and used a flow cytometry-based trafficking assay to monitor the ability of these constructs to support Tspan12 surface expression. While Tspan12 expressed without FZD4 showed low levels on the cell surface, co-expression of Tspan12 with FZD4 resulted in a 4-fold enhancement of Tspan12 expression on the cell surface **(Figure 3B)**. While the ECL1, TM3, and lower hinge chimeras had no or little effect on Tspan12 trafficking, replacement of TM2 with that of FZD10 significantly reduced the amount of Tspan12 on the cell surface, indicating that the interaction of Tspan12 with TM2 of FZD4 is the main determinant of trafficking **(Figure 3B).** TM2 of FZD4 packs against the SEL and TM2 and TM3 of Tspan12, stabilizing a highly bent region between TM2 and the SEL (**Figure 3C, Supplementary Figure 3C**). Tspan12 can bind to Norrin with high affinity without FZD4 present[37], but cannot signal unless it is complexed with FZD4[35]. This unusual trafficking relationship for a tetraspanin may have evolved to prevent apo-Tspan12 from being expressed in high amounts on the cell surface. Apo-Tspan12 would be able to bind to Norrin, but because it is not complexed with FZD4, it would act as a “sink” for Norrin by binding ligand but not being in close enough proximity to FZD4 for efficient signaling.

Tspan12 specifically interacts with FZD4 out of the ten human Frizzled receptors. Analysis of the amino acid sequence conservation of the ten human FZDs revealed a variable patch of residues near the top of TM2 of FZD4 that interacts with TM2 of Tspan12 **(Figure 3D, Supplementary Figure 3D)**. However, the hinge domain and ECL1 of FZD4 are the regions with the most variability, suggesting that though these regions are not essential for trafficking for Tspan12 trafficking, they help drive specificity of Tspan12 to solely FZD4 out of the ten human FZDs.

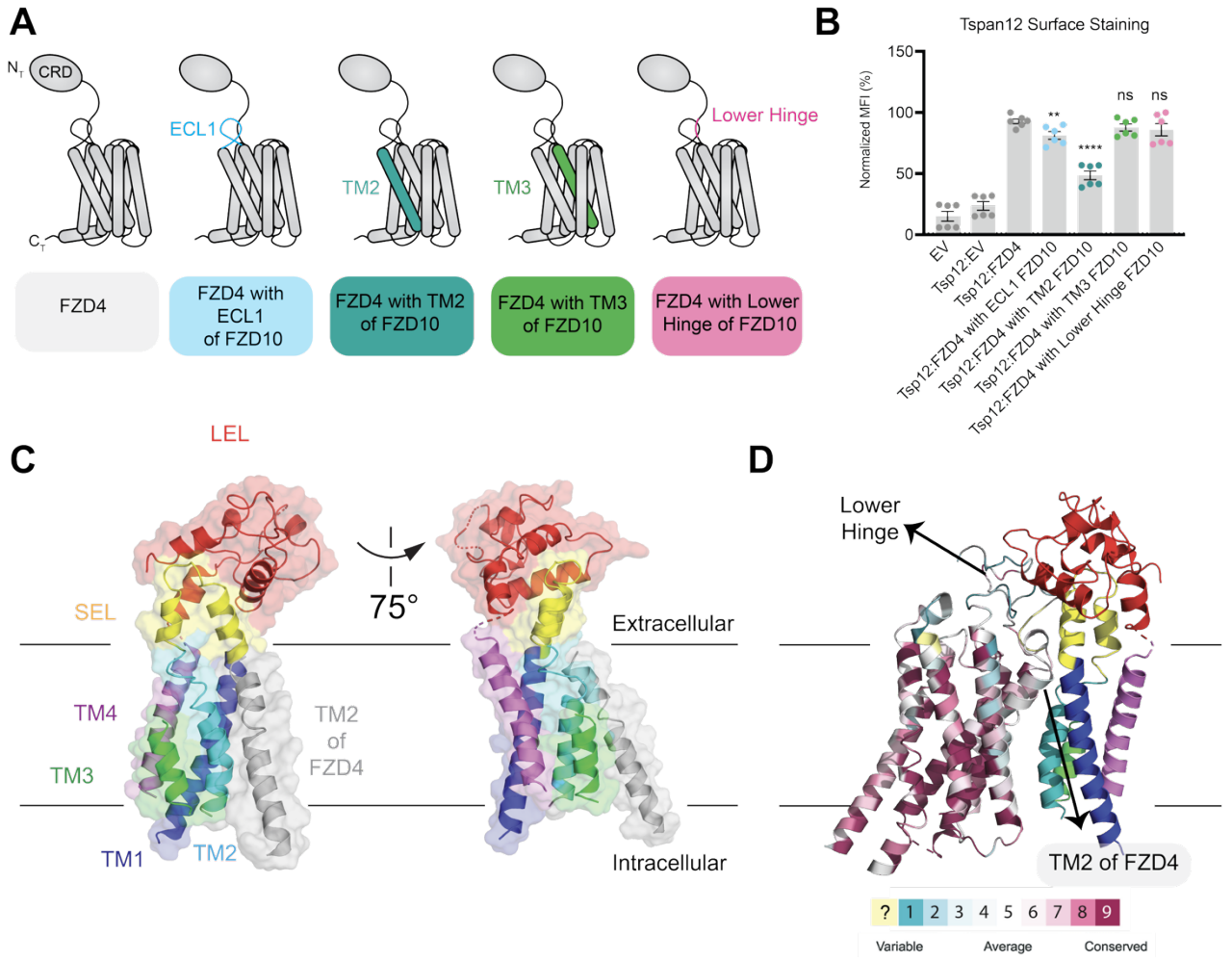

Figure 3: The second transmembrane domain of FZD4 is essential for Tspan12 trafficking to the cell surface. **(A)** Schematic of FZD4-FZD10 chimeras. ECL1, TM2, TM3, or the lower hinge of FZD4 was replaced with that of FZD10. **(B)** Tspan12 trafficking assay with Tspan12 co-transfected with empty vector (EV), FZD4, or a FZD4-FZD10 chimera. Surface Tspan12 was detected by flow cytometry using an Alexa 647-coupled anti-Tspan12 antibody (Biotechne FAB8910R-025). Expression of chimeric FZD constructs is shown in Supplementary Figure 6. **(C)** Atomic representation of Tspan12 bound to FZD4, colored by domain. TM2 of FZD4 (grey) packs against TM2, TM3, and the SEL of Tspan12. **(D)** Structure of FZD4-Tspan12, with Tspan12 colored in grey and FZD4 colored by residue conservation among the 9 human Frizzled paralogs. Residues are colored on a sliding scale from magenta (highly conserved) to blue (poorly conserved). Residues with insufficient information for analysis are colored yellow. Conservation was determined using the Consurf server[54]. In Panel B, error bars represent mean ± SEM of two independent experiments, with three technical replicates each. Statistical analysis was performed in GraphPad Prism using an unpaired t-test, comparing Tspan12:FZD4 to each Tspan12: chimeric FZD4 condition. *p ≤ 0.05, **p ≤0.01, ***p ≤0.001, **** p≤0.0001.

Dynamics of the FZD4-Tspan12 interaction

Recently, a “hand-off” mechanism for Tspan12 function was proposed in which Tspan12 initially promotes the capture of Norrin and then passes off Norrin to FZD4 and LRP5/6, leading to downstream signaling[37]. This model is based on evidence that Tspan12 and LRP5/6 compete for the same binding site on Norrin[37]. Tspan12 binds Norrin with higher affinity (k_d=~10 nM)[37] than LRP5/6 for Norrin (k_d=~450 nM)[13], suggesting that Tspan12 may dissociate from FZD4 after Norrin recognition to facilitate LRP5/6 heterodimerization. We and others have previously shown that tetraspanins are conformationally dynamic, switching between an “open” state[38] and “closed” state[55]. The “open” conformation of the tetraspanin CD81 has a higher affinity for its partner CD19[38,55,56], and we hypothesized that conformational changes in Tspan12 between an open and closed state may facilitate dissociation from FZD4. While the “closed” conformation has a cone-shaped orientation of the transmembrane helices and a large hydrophobic binding pocket capable of binding lipids[55,57], the “open” conformation has a tightly packed four-helix bundle orientation of the TMs, which occludes the lipid binding pocket, and is characterized by a hinge opening of the ectodomain away from the membrane[38,58]. When bound to FZD4, Tspan12 is in the “open” conformation, with a tightly packed orientation of the TMs, similar to the “open” conformation of CD81. **(Figure 4A, 4B)**.

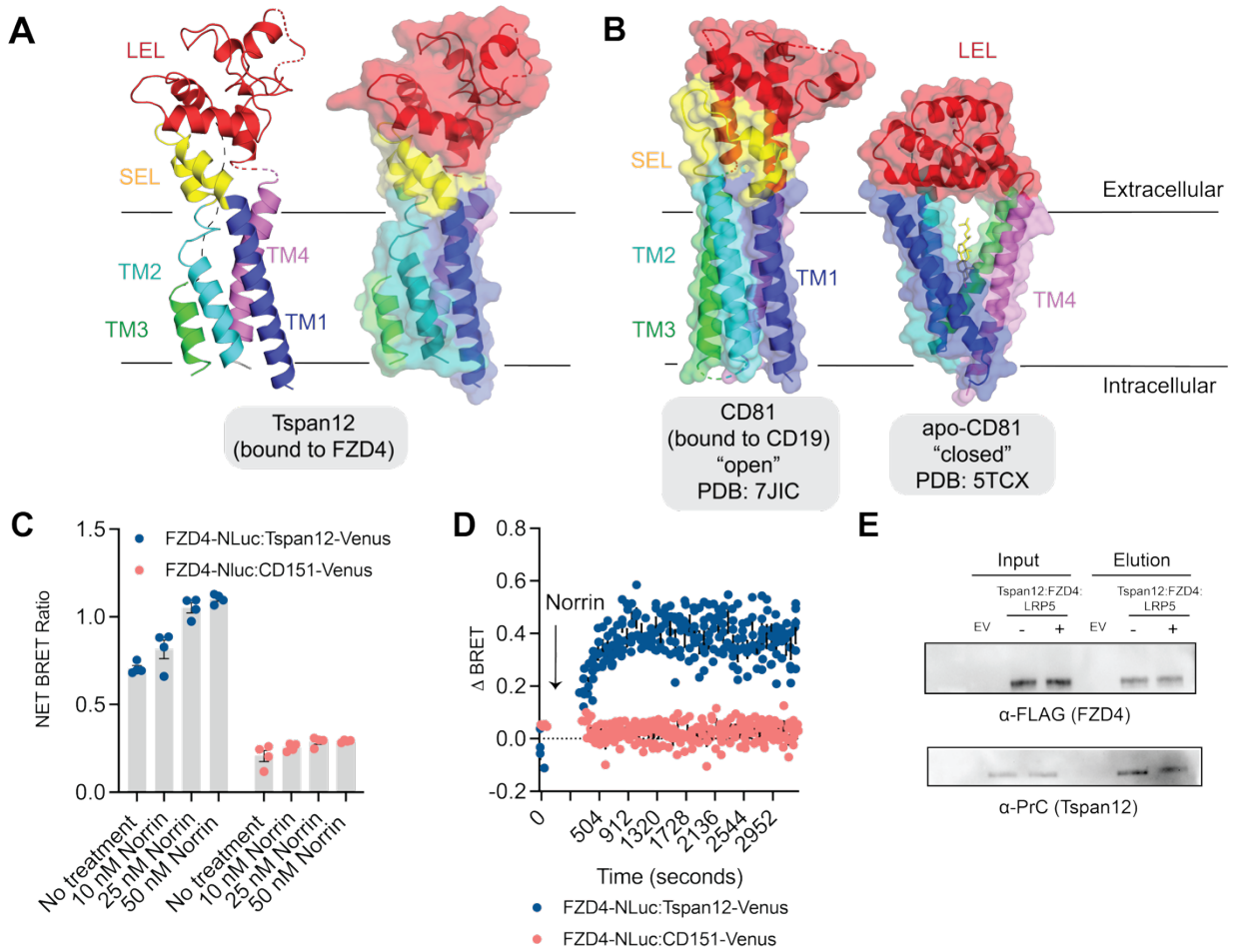

Figure 4: Tspan12 remains as a core component of the FZD4 signaling complex after Norrin recognition. (A) Structure of Tspan12 (bound to FZD4), highlighting an "open" state of Tspan12, with a closely packed four helix bundle orientation of the transmembrane helices. Tspan12 is colored by domain. **(B)** Comparison of "closed" apo-CD81 (right, PDB: 5TCX) with "open" CD19-complexed CD81 (left, PDB: 7JIC). The structures are colored by domain. The "open" conformation refers to an opening of the LEL away from the membrane. **(C)** BRET assay tracking Tspan12-FZD4 proximity. Fixed amounts of FZD4-NLuc were transfected into ΔFZD_{1-10} knockout cells with either CD151-Venus or Tspan12-Venus to assess the change in Tspan12-FZD4 proximity after 5 minutes of treatment with either 10 nM, 25 nM, or 50 nM Norrin. **(D)** Kinetic monitoring of Tspan12-FZD4 proximity upon 10 nM Norrin treatment in ΔFZD_{1-10} knockout cells expressing FZD4-NLuc with either Tspan12-Venus or the negative control, CD151-Venus. **(E)** Pulldown of PrC tagged Tspan12 associated with FLAG tagged FZD4 in untreated cells (-) or after 10 nM Norrin treatment (+) for 15 minutes in ΔFZD_{1-10} knockout cells co-transfected with PrC-Tspan12, FLAG-FZD4, and untagged LRP5. EV: empty vector transfected cells. For BRET experiments in Panels C and D, data are presented as mean ± SEM of five technical replicates.

To determine if Tspan12 dissociates from FZD4 after Norrin recognition, we used a bioluminescence resonance energy transfer (BRET) assay to monitor the association of Tspan12 with FZD4 in cells. We fused the luciferase energy donor NanoLuc (NLuc) to FZD4 and energy acceptor Venus to Tspan12, or a negative control, non-interacting tetraspanin, CD151, using previously reported linkers and insertion sites **(Supplementary Table 2)**[59,60]. When in close proximity (within 10 nm[61]), NLuc and Venus undergo BRET, generating a fluorescent signal. We used this system to ask if the amount of Tspan12 in proximity to FZD4 changes after recognition of Norrin. First, we either left cells untreated or treated cells with either 10, 25, or 50 nM Norrin, and then measured the BRET ratio 5 minutes after Norrin addition **(Figure 4C)**. Importantly, Tspan12-Venus and FZD4-NLuc showed a 4 to 5-fold increase in the BRET ratio compared to our negative control, CD151-Venus, highlighting the ability of the assay to detect the true interaction between FZD4-Tspan12 **(Figure 4C)**. If Tspan12 is dissociating from FZD4 after Norrin treatment, we would expect to see a decrease in the BRET ratio, indicating decreased proximity. However, the BRET ratio was slightly increased following Norrin treatment, suggesting that Tspan12 is not dissociating from FZD4 **(Figure 4C)**. To assess if Tspan12-FZD4 proximity changes over the time course of signaling, we transfected ΔFZD_{1-10} cells with our BRET constructs and LRP5, collected a baseline reading, left the cells untreated or added 10 nM Norrin, and then collected a time course of the BRET signal over a period of approximately 55 minutes **(Figure 4D)**. Again, we saw the BRET ratio was slightly increased and remained constant during our entire data collection period, indicating that Tspan12 remains as a core component of the FZD4 complex after ligand recognition. Moreover, co-immunoprecipitation of Tspan12 and FZD4 in cells with or without Norrin treatment showed similar amounts of Tspan12 pulled down, providing further evidence that Tspan12 remains associated with FZD4 **(Figure 4E)**. These data are consistent with a prior report that Tspan12 co-localizes with FZD4-Norrin-LRP5 signaling complex at the cell surface and in endosomes[62].

DISCUSSION

Here, we report the structure of the co-receptor Tspan12 bound to FZD4, showing that Tspan12 and FZD4 form a direct complex in the absence of Norrin. Tspan12 engagement of FZD4 enables both higher affinity binding to Norrin and recognition of a wider range of Norrin concentrations. Tspan12 remains a core component of the FZD4-LRP5/6 signaling complex after Norrin recognition. This raises a fundamental question: if Tspan12 is not dissociating from FZD4, how is LRP5/6 able to be recruited to the complex? A potential mechanism is that Tspan12 remains incorporated in the Norrin-FZD4-LRP5/6 complex, with Tspan12 and LRP5/6 each binding to opposite Norrin protomers. Although Norrin is a disulfide-linked homodimer that is overall two-fold symmetric, the cysteine knot fold of Norrin results in distinct spatial orientations of each protomer, breaking perfect symmetry **(Figure 5A).** In the second Norrin protomer, the Tspan12 binding site is rotated approximately 90° **(Figure 5B).** The AlphaFold-Multimer model of Norrin bound to two Tspan12 molecules shows that this orientation results in the second Tspan12 molecule being rotated 90° perpendicular to the membrane plane, which would be physiologically incompatible with binding (**Supplementary Figure 7)**. Based on our BRET data showing no dissociation of FZD4 and Tspan12 upon Norrin recognition and our pulldown showing no change in the amount of Tspan12 associated with FZD4 upon Norrin treatment, we propose a model in which LRP5/6 binds to the opposite protomer of Norrin, leading to the formation of a stable Tspan12-FZD4-LRP5/6 signaling complex **(Figure 5C)**. Although biochemical experiments have shown that LRP6 and Tspan12 compete for the same binding site on Norrin[37], it is also possible that their binding sites are only partially overlapping, which would enable recruitment of LRP5/6 to both protomers on Norrin, and the overall stoichiometry of Norrin binding to the complex is not known.

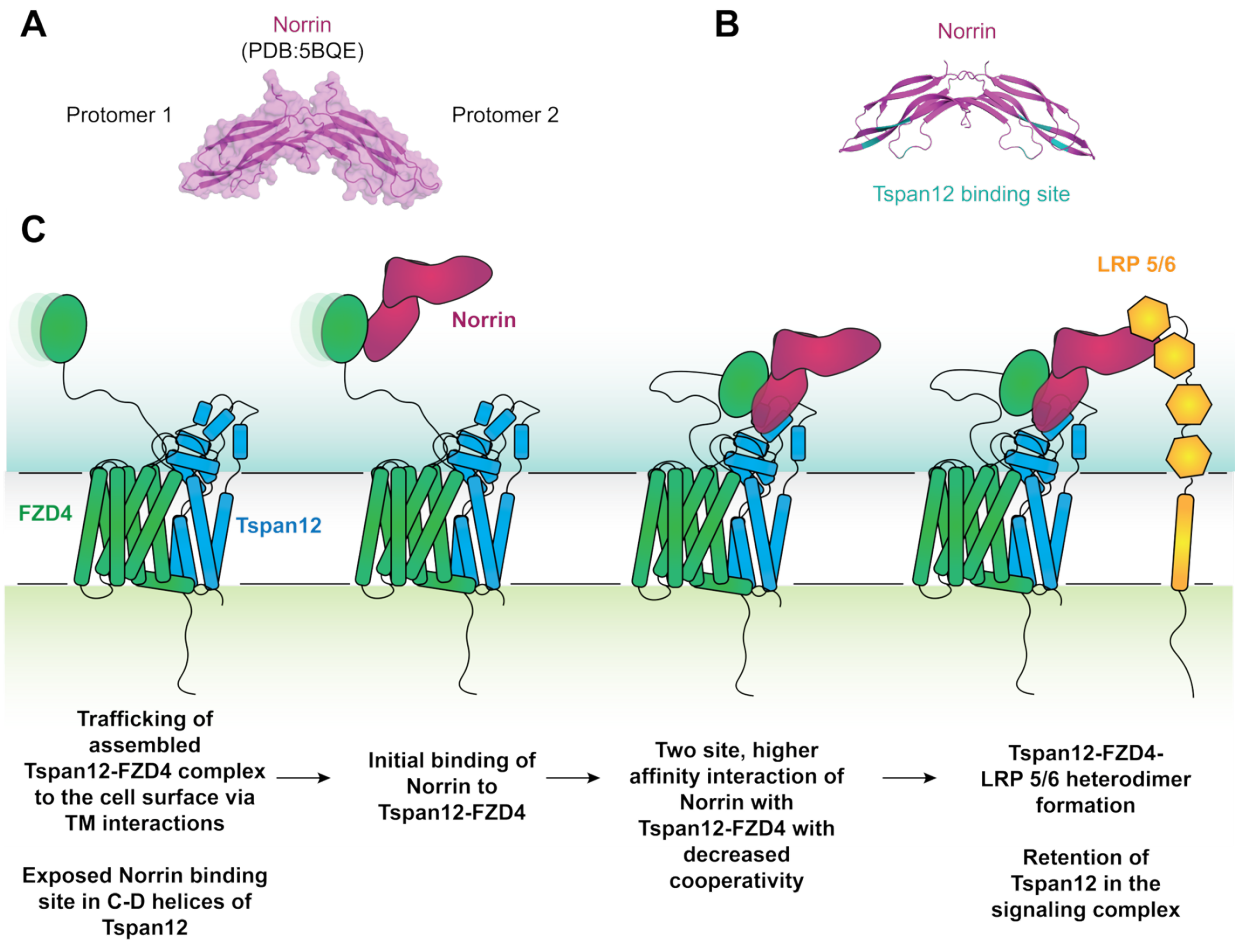

Figure 5: Proposed model for Tspan12 assembly into the Norrin-FZD4-LRP5/6 signaling complex. (A) Crystal structure of Norrin (PDB:5BQE). **(B)** Tspan12 binding site[37] mapped onto the surface of Norrin, highlighting distinct spatial orientations of the Tspan12 binding site on each protomer. Residues within 5 Å of Tspan12 in the Tspan12-Norrin AlphaFold3 model are colored in teal. **(C)** Proposed model for incorporation of Tspan12 into the Norrin-FZD4-LRP5/6 signaling complex. Tspan12 is trafficked to the cell surface with FZD4 and exists in complex with FZD4 before Norrin recognition. Norrin engages in a two-site interaction with Tspan12-FZD4 to recruit LRP5/6 into a Tspan12-FZD4-LRP5/6-Norrin signaling complex.

Wnts contact FZDs through a highly conserved two-site mechanism, positioning “thumb” and “finger” domains on opposite sides of the CRD[6]. Why Wnts need a two-site mode of engagement is debated, but one model is that it provides specificity, avidity, and optimally orients the Wnt ligand for LRP5/6 engagement[6,65]. Importantly, Norrin contacts the CRD of FZD4 at a single site[63,64], suggesting a role for Tspan12 may be to provide an additional second binding site

to facilitate LRP5/6 recruitment and downstream signaling. The C-D helices of Tspan12 are anchored close to the membrane in our structure, and our results suggest that one role of Tspan12 may be to prevent Norrin from diffusing away by providing avidity through its additional binding site and to restrain the motion of Norrin bound to the highly dynamic CRD-Hinge region of FZD4, facilitating proper orientation of Norrin to increase the likelihood of LRP5/6 recruitment. Structural characterization of the native FZD4-Tspan12-LRP5/6-Norrin complex and Wnts in complex with full-length FZDs and LRP5/6 will be needed to answer this question and will remain an important area of future investigation.

The partnership between FZD4 and Tspan12 represents an important, heretofore unappreciated function of tetraspanins in the direct regulation of receptor signaling. Tetraspanins are recognized as "molecular facilitators"[21], acting as chaperones to traffic partner proteins to the cell surface and regulate their plasma membrane localization[22,52]. However, they are not appreciated as a family of membrane proteins that directly signal or bind to endogenous ligands. The finding that Tspan12 directly binds to Norrin with high affinity[37] and our findings that Tspan12 modulates the binding properties of FZD4 to Norrin and remains a component of the active Norrin-FZD4-LRP5/6 signaling complex highlight an important role for tetraspanins in direct regulation of signaling, rather than simply functioning as molecular chaperones in the membrane. 10 out of 33 human tetraspanins have an intracellular tail, indicating that more tetraspanins than appreciated may play a direct role in signal transduction. The 59 amino acid C-terminal cytoplasmic tail of Tspan12 contains several putative phosphorylation sites, suggesting it may play a role in signaling by scaffolding the recruitment of intracellular signaling molecules. Other tetraspanins have been shown to scaffold phosphoiniositide kinases and protein kinase C[66,67]. An important area of future studies will be characterizing which signaling molecules bind to the intracellular tail of Tspan12 and their role in amplification of β-catenin signaling, and to characterize whether any other tetraspanins directly bind an endogenous ligand within their ectodomain

Modulation of β-catenin signaling is an area of active therapeutic investigation for cancer, degenerative diseases, and diseases related to blood vessel angiogenesis, like FEVR[2,68]. Mutations in Tspan12 are found in approximately 5-10% of FEVR patients[18,19,29–33]. Mapping known missense mutations found in FEVR patients onto the structure of FZD4-Tspan12 revealed that these mutations do not map to the Tspan12-FZD4 binding interface **(Supplementary Figure 8)**, suggesting instead that these mutations likely decrease Norrin binding or affect protein quality or folding. Targeting the β-catenin pathway remains challenging due to toxicity stemming from broad inhibition of β-catenin signaling. While FZD4 and LRP5/6 are widely expressed throughout the body, Tspan12 is primarily expressed in the retina[35], offering a potentially powerful way to specifically modulate Norrin signaling for the treatment of diseases of retinal hypo-vascularization, such as FEVR, or for ocular diseases associated with retinal hyper-vascularization, such as diabetic retinopathy. Tspan12 antibodies have been reported that inhibit Norrin signaling and decrease angiogenesis[69]. Our results suggest that because Tspan12 forms a direct complex with FZD4, modulates how FZD4 responds to Norrin, and stays engaged with the LRP5 signaling complex, antibodies that either block the Norrin binding site on Tspan12 or stabilize the interaction of Norrin with Tspan12 may offer new ways to treat diseases characterized by retinal hyper-vascularization and hypo-vascularization, respectively.

ACKNOWLEDGEMENTS

This work was funded by an NIH grant DP5OD036136 and a UCSF Sandler Fellowship to K.J.S, and an NIH IMSD training grant 5R25GM056847-25 and Achievement Rewards for College Scientists (ARCS) scholarship to K.A.E.A. We thank members of the Susa and Manglik labs, Dr. Elise Bruguera for helpful discussions, the Manglik lab for the use of equipment, and Dr. Meredith Anne Skiba for the anti-F_{ab} nanobody. We thank Dr. Julia Maria Rogers, Dr. Edward Harvey, and Dr. Aashish Manglik for feedback on the manuscript. Cryo-EM data were collected at the Cryo-EM facility at the University of California, San Francisco. We thank Glenn Gilbert for helpful

comments and assistance during grid screening and data collection. We thank Benoit Vanhollebeke for generating and generously sharing ΔFZD_{1-10} HEK293T cells[70].

AUTHOR CONTRIBUTIONS

K.J.S. designed and conceived of the project. A.J.G., P.P.P., K.A.E.A, and K.J.S. designed experiments. A.J.G. and K.J.S. prepared the sample for cryo-EM, and A.J.G., K.J.S., and P.P.P. collected and processed cryo-EM data. P.P.P. and K.J.S. performed model building and refinement. A.J.G., K.A.E.A., and K.J.S. performed cell-based assays. K.J.S. wrote the manuscript with input from all authors. K.J.S. supervised the work and provided financial funding.

COMPETING INTERESTS STATEMENT

The authors declare no competing interests.

DATA AND MATERIALS AVAILABILITY

Materials will be made available upon request. Protein Data Bank (PDB) IDs of the FZD4-Tspan12-BRIL F_{ab} model and map are 9YEV and EMD-72864, respectively.

METHODS

Design of FZD4-Tspan12 fusion protein

The FZD4-Tspan12 fusion was cloned into a doxycycline-inducible pcDNA3.1 (+) tet/zeo vector with an N-terminal haemagglutinin signal sequence followed by a FLAG epitope tag. Residues 37-537 of human FZD4 (full length, excluding the endogenous signal sequence) were connected to full-length human Tspan-12 (residues 2-305) using a GGGSx4 linker. The linker length was engineered to be long enough in length to ensure tethering of Tspan12 would not enforce Tspan12 engagement on one side of FZD4. For the BRIL FZD4-Tspan12 construct, BRIL replaced ICL3 (residues 416-427) of FZD4 using linkers derived from the A_{2A} adenosine receptor (ARRQL between residue 415 and the N-terminus of BRIL, and ARSTL between the C-terminus of BRIL

and residue 428). Tspan12 was linked to FZD4-BRIL with a GGGSx4GGSx3 linker. BRIL insertion was guided by monitoring the rigidity of the BRIL linkage using AlphaFold3, and the insertion linkage was modified using the strategy for a previously reported FZD5-BRIL fusion[40].

Protein expression and purification of FZD4-BRIL-Tspan12 complexes

The FZD4-Tspan12 fusion protein was expressed in Expi293F TetR cells containing a stably integrated tetracycline repressor grown in Expi293 (Thermo) media supplemented with 20 µg/mL Blasticidin (Invivogen). 500 mL of Expi293F TetR cells were grown to a density of approximately 2.8 x 10^6 cells/mL and then transiently transfected with 0.4 mg of DNA and FectoPro transfection reagent (Polyplus) at a 1:1 DNA/FectoPro ratio. 24 hours after transfection, the cells were fed 3 mM valproic acid sodium salt (Sigma-Aldrich) and 4.5 mL of 45% D-(+)-Glucose solution (Sigma-Aldrich). 24 hours later, transfected cells were induced with 5 mL 0.4 mg/mL doxycycline hyclate dissolved in HBSS. 24 hours after induction, cells were harvested by centrifugation at 4000 g for 10 minutes at 4°C. The mass of the pellet was recorded and then flash frozen and stored at -80°C until purification.

After the frozen cells were thawed, cells were lysed by osmotic shock in 150 mL 20 mM HEPES pH 7.4, 2 mM magnesium chloride, 2 mg/mL iodoacetamide (Sigma Aldrich), and 1:100,000 (v:v) benzonase nuclease (Sigma Aldrich). Lysed cells were centrifuged at 18,000xg for 20 min. FZD4-Tspan12 was then extracted from the pellet using a glass dounce tissue grinder in 150 mL solubilization buffer containing 20 mM HEPES pH 7.4, 250 mM NaCl, 10% (v/v) glycerol, 1% (w/v) n-Dodecyl-β-D-Maltoside (DDM - Anagrade; Anatrace), 0.1% (w/v) cholesterol hemisuccinate (CHS;Steraloids), and 2 mg/mL iodoacetamide. The sample was stirred for 2 hours at 4°C and then centrifuged at 20,000xg for 30 minutes at 4°C. Supernatant supplemented with 2 mM calcium chloride was filtered through a glass microfiber prefilter and loaded by gravity flow onto 2.5 mL of M1 anti-FLAG antibody affinity resin. The resin was washed with 100 mL of buffer containing 20

mM HEPES pH 7.4, 150 mM NaCl, 2 mM $CaCl_2$, 0.1% DDM, and 0.01% CHS, and then 100 mL of buffer containing 2 mM $CaCl_2$, 150 mM NaCl, 20 mM HEPES pH 7.4, 0.05% GDN (Anatrace), and 0.005% CHS. Bound protein was eluted in 20 mL buffer containing 20 mM HEPES pH 7.4, 50 mM NaCl, 0.05% GDN, and 0.005% CHS, 5 mM EDTA, and 0.2 mg/mL FLAG peptide. The elution was concentrated in a 100k MWCO centrifugal filter and then complexed to anti-BRIL Fab and anti-Fab nanobody (Nb). FZD4-Tspan12 was incubated with anti-BRIL Fab and anti-Fab Nb at a 1:1.4:2 molar ratio, respectively, on ice for 1 hour. The complex was then purified by size exclusion chromatography (SEC) on a Superose 6 column (GE Healthcare) in buffer containing 20 mM HEPES pH 7.4, 150 mM NaCl, 0.05% GDN, and 0.005% CHS. Immediately after the FZD4-Tspan12-Fab-Nb complex eluted from the S6 column, two fractions were concentrated to 3.65 mg/mL using a 100k MWCO centrifugal filter and then applied to grids. Purity and monodispersity of the sample for cryo-EM were evaluated by SDS-PAGE and SEC **(Supplementary Figure 1)**.

Purification for anti-BRIL Fab

The heavy and light sequences of the previously described anti-BRIL Fab (BAG2)[43] were cloned into the pTarget and p261040 (Atum) vectors, respectively. A set of previously described stabilizing mutations (SSASTKG replaced with FNQIKG) were introduced into the hinge region of the heavy chain to increase its rigidity[71]. The heavy and light chains were co-expressed in Expi293F cells (Thermo Fisher, Catalog number A14527). 500 mL of Expi293F cells maintained in Expi293 expression media were grown to a density of 2.8 x 10^6 cells/mL and then transiently co-transfected with heavy and light chain DNA at a 1:1 (w:w) ratio (0.40 mg total DNA) and FectoPro transfection reagent (Polyplus) at a 1:1 (w:w) DNA/FectoPro ratio. Approximately 20 hours after transfection, 3 mM valproic acid sodium salt (Sigma-Aldrich) and 4.5 mL of 45% D-(+)-Glucose solution (Sigma-Aldrich) were added to the cultures. Transfected cells were cultured for 5 days to produce protein, and then the media was collected and separated from the cells by

centrifugation at 4000xg for 15 minutes at 4°C. The cultured media was loaded onto 2.5 mL CaptureSelect CH1-XL Affinity Matrix (ThermoScientific) resin pre-equilibrated with buffer containing 20 mM HEPES pH 7.4, 150 mM NaCl (HBS). The resin was washed with 100 mL HBS, and then the bound protein was eluted in 15 mL 100 mM citrate buffer pH 3.0. Elution fractions were immediately neutralized with 1 M HEPES pH 8, concentrated using a centrifugal filter to approximately 2 mL final volume (17 mg/mL) and dialyzed overnight into phosphate buffered saline (PBS). The purity of the eluted protein was assessed on an SDS-PAGE Coomassie-stained gel, and small aliquots were flash frozen in liquid nitrogen and stored at -80 °C until use. Before complexing to FZD4-Tspan12, anti-BRIL Fab and anti-Fab nanobody were buffer-exchanged into buffer containing 20 mM HEPES pH 7.4, 150 mM NaCl, 0.05% GDN, and 0.005% CHS (w/v).

Cryo-EM sample preparation and data collection

Samples for cryo-EM were prepared on Quantifoil holey carbon film-coated 400 mesh gold grids (Electron Microscopy Sciences, R1.2/1.3, Cat: N1-C14nAu40-01). Grids were glow-discharged before the application of 3.5 µL of the sample (3.6 mg/mL). After blotting for 5.5 s with a blot force of 5, the grids were plunge-frozen in liquid ethane using a FEI Vitrobot Mark IV (FEI, Hillsboro) with 100% chamber humidity at 22°C.

Cryo-EM data processing and model building

Grids were loaded onto a 2nd-generation Titan Krios, and data collection was automated through Serial EM[72]. Collection parameters are shown in Supplementary Table 1. Micrographs were imported into CryoSPARC v4.5.3[73] and processed as shown in Supplementary Figure 2A to resolve the FZD4-BRIL-Tspan12 fusion construct in complex with BRIL fab and anti-fab nanobody to 3.38 Å (best overall map) and 3.55 Å (Tspan12 focused map) using non-uniform refinement[74]. The Tspan12-focused map was further processed to 3.4 Å using Deep EMhancer[75,76].

Model building was carried out using both non-uniform refinement and deepEMhancer maps overlayed in Coot[77]. The AlphaFold3 models of Tspan12 and FZD4-BRIL and the atomic coordinates of the BRIL Fab and anti-Fab nanobody (PDB: 6WW2 were manually fitted into the density map using ChimeraX to generate a starting model[78]. The transmembrane domains and extracellular domains of Tspan12 docked into the density separately to allow for fitting. The coordinates were then manually rebuilt using Coot[77]. TM4 of Tspan12 was poorly resolved and modeled as polyalanine, and side chains with poor density within the Tspan12 LEL or TMs with poor density were truncated to Cβ. All models were refined in Phenix realspace refine[79,80] with secondary structure restraints against the 3.4. map from non-uniform refinement in cryoSPARC. The final models were evaluated by MolProbity and EMRinger[81,82]. Statistics of the map reconstruction and model refinement are presented in Supplementary Table 1. Structural biology applications used in this project (other than CryoSPARC) were compiled and configured by SBGrid[83]. Structural depictions were creations through UCSF ChimeraX.

Tspan12 trafficking assay

2 mL of Expi293F TetR cells were seeded at 2.8E6 cells/mL in a 6 well plate and then transfected using FectoPro (PolyPlus) with either: **1)** 1.5 ug empty pcDNA3.1tet/zeo (+) vector, **2)** 0.75 ug empty pcDNA3.1tet/zeo (+) vector and 0.75 ug pcDNA3.1tet/zeo (+) Tspan12, **3)** 0.75 ug pcDNA3.1tet/zeo (+) FLAG-FZD4 (full-length) and 0.75 ug pcDNA3.1tet/zeo (+) Tspan12 (full-length), or **4)** 1.5 ug FLAG-FZD4-Tspan12 fusion. 24 hours after transfection, 3 mM valproic acid sodium salt (Sigma-Aldrich) and 18 µL of 45% D-(+)-Glucose solution (Sigma-Aldrich) were added to the cultures. 24 hours later, receptor expression was induced with 20 uL of 0.4 mg/mL doxycycline hyclate dissolved in HBSS. 24 hours after induction, cells were harvested by centrifugation at 4000 g for 10 minutes at 4°C. Approximately 500,000 cells were added to each well of a V-bottom 96-well plate (Costar), and cells were washed with cold PBS. Cells were then

incubated on ice for 30 minutes with 10 µg/mL Alexa 488-anti-M1 FLAG (hybridoma) and Alexa 647-anti-Tspan12 (Biotechne Catalog #: FAB8910R) in 20 mM HEPES buffer pH 7.4, containing 150 mM NaCl, 2 mM CaCl2, and 0.1% BSA. Cells were washed twice with cold PBS and analyzed on an Agilent Novocyte 3000.

Expression and purification of MBP-Norrin

MBP-Norrin was expressed and purified as previously described[37,59] . MBP-3C-Norrin (33-133)-1D4 with an IL2 signal sequence was cloned into the pFUSE vector (Invitrogen). 500 mL of Expi293 cells were grown to a density of approximately 2.8 x 10^6 cells/mL and then transiently transfected with 0.4 mg of DNA and FectoPro transfection reagent (Polyplus) at a 1:1 DNA/FectoPro ratio. 24 hours after transfection, the cells were fed 3 mM Valproic acid sodium salt (Sigma-Aldrich) and 4.5 mL of 45% D-(+)-Glucose solution (Sigma-Aldrich). 9 days after transfection, the culture was harvested by centrifugation at 4000x g for 15 minutes at 4°C. The culture supernatant was loaded onto 2 mL amylose resin (New England Biolabs). The resin was washed with 5 column volumes of buffer containing 20 mM HEPES pH 8, 150 mM NaCl, 1 mM EDTA, and 5% glycerol. Bound protein was eluted in 20 mL of buffer containing 20 mM HEPES pH 8, 150 mM NaCl, 1 mM EDTA, 5% glycerol, and 10 mM maltose. Eluted MBP-Norrin was concentrated using a 30 MWCO spin concentrator (Amicon), and concentrated was loaded on a Superdex 200 Increase 10/300 GL in buffer containing 20 mM HEPES pH 8, 150 mM NaCl, 1 mM EDTA, and 5% glycerol. Peak fractions were pooled, concentrated to approximately 1 mg/mL, flash frozen, and frozen in 25 µL aliquots at -80°C until use **(Supplementary Figure 9)**. MBP-Norrin was validated in FZD4 binding assays before use.

MBP-Norrin binding assays

2 mL of Expi293F TetR cells were seeded at 2.8E^6 cells/mL in a 6 well plate and then transfected using FectoPro (PolyPlus) with either mock transfected with 1.5 µg empty pcDNA3.1tet/zeo (+) or

1.5 ug of FLAG-apo-FZD4, FLAG-FZD4-BRIL-Tspan12, or a chimeric FLAG-FZD4-BRIL-Tspan12. 24 hours after transfection, 3 mM valproic acid sodium salt (Sigma-Aldrich) and 18 µL of 45% D-(+)-Glucose solution (Sigma-Aldrich) were added to the cultures. 24 hours later, receptor expression was induced with 20 µL of 0.4 mg/mL doxycycline hyclate dissolved in HBSS. 24 hours after induction, cells were harvested by centrifugation at 1,000xg and resuspended in cold phosphate buffered saline (PBS). The cells were then counted, and 100,000 cells were added to each well of a v-bottom 96 well plate (Grenier Bio). Cells were washed again with 100 µL cold PBS and then were incubated with different concentrations of either the 1D4-tagged MBP-Norrin, secondary antibody alone (anti-1D4-488), M2-FLAG-488 to quantify receptor expression level, or buffer alone for thirty minutes at 4°C[36,71]. Following another PBS wash, cells were incubated with 2 µg/mL anti-Rho1D4-Alexa Fluor 488 antibody for 30 minutes at 4°C to detect Norrin binding. After secondary antibody incubation, cells were washed twice more with PBS and were analyzed by flow cytometry using a Novocyte 3000 (Agilent). In detail, live/dead gates were set using SSC-A versus FSC-A and singlet gates using FSC-H versus FSC-A, and fluorescence intensity at 488 nm was recorded in the doubly gated population. Median fluorescence intensity (MFI) at 488 nm was plotted in GraphPad Prism as an assessment of MBP-Norrin binding to cells. For EC50 calculations, non-specific signal was subtracted (MFI in the mock condition treated with the corresponding MBP-Norrin concentration), and then values were normalized for receptor expression, detected with an anti-FLAG-488 antibody. Curve fitting was performed in Prism (GraphPad, v10) to a log (agonist) vs. response four-parameter model, with no constraints on Hill Slope, EC50, or top and bottom values.

BRET assays

ΔFZD_{1-10} HEK293T cells were used for all BRET experiments. White 96-well tissue-culture treated plates (Revity) were precoated with 50 µL/well of a 0.1 mg/mL poly-D-lysine (Sigma) and incubated at room temperature for 20 minutes. The coating solution was aspirated and washed

once with 200 µL/well of DPBS, and the plate was dried for 20 minutes in the tissue culture hood before seeding cells. ΔFZD_{1-10} HEK293T cells were trypsinized and diluted to $0.4E^5$ cells/mL. 1 mL of cells at $0.4E^5$/mL were then transfected in suspension. Acceptor: donor transfection ratios were pre-determined from acceptor: donor titration experiments to determine the signal plateau and fold increase over the CD151-Venus negative control. For transfections, Tube A contained 40 µL opti-MEM, 20 ng FZD4-NLuc, 100 ng Tspan12-Venus or CD151 Venus, or 0 ng of a Venus construct as a background control, and 20 ng untagged LRP5. Empty pcDNA3.1 vector was used to bring to a final concentration of DNA to 1,000 ng. Tube B contained 49 µL Opti-MEM and 1 µL Lipofectamine 2000. Tubes A and B were incubated separately for 5 minutes, and then added together and incubated at room temperature for 10 minutes. The transfection mix was added dropwise to 1 mL of cells at $0.4E^5$/mL, 100 µL of the cell-transfection mix was added to each well of the poly-D-lysine-coated 96-well plate. Approximately 24 hours after transfection, cells were washed once with 200 µl of HBSS and then kept in HBSS. 10 µL of furimazine (Promega) (final dilution at 1:1000) was added to a final volume of 90 µL, and 5 min after furimazine addition, luminescence was read three times for a baseline reading. Subsequently, 10 µL of Norrin at a final concentration of either 10 nM or 50 nM (in HBSS) was added to a final volume of 100 µL, and luminescence reading was continued 44 times for a total of 54.8 minutes. All measurements were performed at 37°C using a ClarioStar plate reader. BRET experiments were performed with five replicates.

Tspan12 Pulldown

ΔFZD_{1-10} HEK293T cells were seeded at $0.3E^6$ cells/mL in 10 mL DMEM with 10% FBS (Fisher Scientific SH3007003HI) and 1% Pen-Strep (Thermo Scientific 15140122). Approximately 12 hours later, media was replaced with 10 mL DMEM with 2% FBS and no Pen/Strep. Per 10 cm^3 plate, cells were transfected with 1.2 ug DNA, at a ratio of 1:1.5:4 FZD4:LRP5:Tspan12, or 1.2 µg empty vector (pcDNA3.1), and 40 µL lipofectamine 2000 in 1.5 mL opti-MEM. The FZD4 was

N-terminally FLAG tagged, Tspan12 was N-terminally Protein C (PrC) tagged, and LRP5 was untagged. The transfection mix was incubated for 15 minutes at room temperature and then added dropwise to the cells. The next day, the media was replaced with DMEM with 10% FBS and 1% Pen-Strep. 48 hours after transfection, cells were serum starved for 1 hour in DMEM with no FBS and then treated with 10 nM of Norrin for 15 minutes or left untreated. Cells were harvested in 2 mL cold PBS with 5 mM EDTA, pelleted at 4000xg for 10 minutes at 4°C. The pellet was lysed by osmotic shock in 20 mM HEPES pH 7.4, 2 mM $MgCl_2$, 2 mg/mL iodoacetamide, and 1:100,000 v:v benzonase. Tubes were rotated for 30 minutes at 4°C and then spun at 16,000xg for 15 minutes at 4°C. The pellet was resuspended in solubilization buffer (1% (w/v) DDM/0.1% CHS buffer, 20 mM HEPES pH 7.4, 250 mM NaCl, 10% glycerol, 2 mg/mL iodoacetamide) and rotated for 2 hours at 4°C. Cells were pelleted at 20,000 g for 30 minutes at 4°C and then added to 25 µL of M2 magnetic FLAG beads (Sigma, M8823). The samples were rotated for 2 hours in the cold room, and then each tube was washed 3x with 1 mL 0.1% (w/v) DDM 0.01% CHS buffer, 20 mM HEPES pH 7.4, 150 mM NaCl. Bound proteins were eluted directly from the beads in 250 µL SDS loading dye.

10% inputs and 10% eluates were run on a non-reducing SDS-PAGE gel, and the protein was transferred to a nitrocellulose membrane. The membrane was then gently rocked in TBST (0.1% Tween-20 in Tris-buffered-saline) blocking buffer with 5% (w/v) Bovine Serum Albumin (BSA) (Fisher Scientific BP9706100) at room temperature for 1 hour. The blocked membrane was cut and then incubated in TBST with 1% (w/v) BSA containing either FLAG-HRP conjugate antibody (Cell Signaling 86861S; 1:1,000 dilution) or anti-Protein C (PrC) tag antibody (Cell Signaling 68083; 1:1000 dilution). Antibody incubations were performed overnight at 4°C with shaking. The Tspan12-PrC blot was incubated with anti-Rabbit IgG HRP Conjugate (Cell Signaling 7074S; 1:5,000) in TBST containing 1% (w/v) BSA. Secondary antibody incubation was performed for 1 hour at room temperature with shaking. Prior to chemiluminescent detection, blots were washed

with TBST three times for 10 min each time. Western blots were developed with Western Lightning Plus-ECL, Enhanced Chemiluminescence Detection Kit (PerkinElmer).

REFERENCES

1. Wodarz, A. & Nusse, R. MECHANISMS OF WNT SIGNALING IN DEVELOPMENT. *Annu. Rev. Cell Dev. Biol.* **14**, 59–88 (1998).
2. MacDonald, B. T., Tamai, K. & He, X. Wnt/β-Catenin Signaling: Components, Mechanisms, and Diseases. *Dev. Cell* **17**, 9–26 (2009).
3. Schulte, G. & Bryja, V. The Frizzled family of unconventional G-protein-coupled receptors. *Trends Pharmacol. Sci.* **28**, 518–525 (2007).
4. Bhanot, P. *et al.* A new member of the frizzled family from Drosophila functions as a Wingless receptor. *Nature* **382**, 225–230 (1996).
5. Dann, C. E. *et al.* Insights into Wnt binding and signalling from the structures of two Frizzled cysteine-rich domains. *Nature* **412**, 86–90 (2001).
6. Janda, C. Y., Waghray, D., Levin, A. M., Thomas, C. & Garcia, K. C. Structural Basis of Wnt Recognition by Frizzled. *Science* **337**, 59–64 (2012).
7. Tamai, K. *et al.* LDL-receptor-related proteins in Wnt signal transduction. *Nature* **407**, 530–535 (2000).
8. Wong, H.-C. *et al.* Direct Binding of the PDZ Domain of Dishevelled to a Conserved Internal Sequence in the C-Terminal Region of Frizzled. *Mol. Cell* **12**, 1251–1260 (2003).
9. Bilic, J. *et al.* Wnt induces LRP6 signalosomes and promotes dishevelled-dependent LRP6 phosphorylation. *Science* **316**, 1619–1622 (2007).
10. Rim, E. Y., Clevers, H. & Nusse, R. The Wnt Pathway: From Signaling Mechanisms to Synthetic Modulators. *Annu. Rev. Biochem.* **91**, 571–598 (2022).
11. Chen, Z. Y. *et al.* Isolation and characterization of a candidate gene for Norrie disease. *Nat. Genet.* **1**, 204–208 (1992).
12. Berger, W. *et al.* Isolation of a candidate gene for Norrie disease by positional cloning. *Nat. Genet.* **1**, 199–203 (1992).
13. Ke, J. *et al.* Structure and function of Norrin in assembly and activation of a Frizzled 4–Lrp5/6 complex. *Genes Dev.* **27**, 2305–2319 (2013).
14. Meindl, A. *et al.* Norrie disease is caused by mutations in an extracellular protein resembling C-terminal globular domain of mucins. *Nat. Genet.* **2**, 139–143 (1992).
15. Niehrs, C. The complex world of WNT receptor signalling. *Nat. Rev. Mol. Cell Biol.* **13**, 767–779 (2012).
16. Xu, Q. *et al.* Vascular development in the retina and inner ear: control by Norrin and Frizzled-4, a high-affinity ligand-receptor pair. *Cell* **116**, 883–895 (2004).
17. Ye, X., Wang, Y. & Nathans, J. The Norrin/Frizzled4 signaling pathway in retinal vascular development and disease. *Trends Mol. Med.* **16**, 417–425 (2010).
18. Nikopoulos, K. *et al.* Overview of the mutation spectrum in familial exudative vitreoretinopathy and Norrie disease with identification of 21 novel variants in FZD4, LRP5, and NDP. *Hum. Mutat.* **31**, 656–666 (2010).
19. Jia, L.-Y. & Ma, K. Novel Norrie disease gene mutations in Chinese patients with familial exudative vitreoretinopathy. *BMC Ophthalmol.* **21**, 84 (2021).
20. Junge, H. J. *et al.* TSPAN12 Regulates Retinal Vascular Development by Promoting Norrin- but Not Wnt-Induced FZD4/β-Catenin Signaling. *Cell* **139**, 299–311 (2009).
21. Maecker, H. T., Todd, S. C. & Levy, S. The tetraspanin superfamily: molecular facilitators. *FASEB J.* **11**, 428–442 (1997).

22. Hemler, M. E. Tetraspanin functions and associated microdomains. *Nat. Rev. Mol. Cell Biol.* **6**, 801–811 (2005).
23. Susa, K. J., Kruse, A. C. & Blacklow, S. C. Tetraspanins: structure, dynamics, and principles of partner-protein recognition. *Trends Cell Biol.* **34**, 509–522 (2024).
24. Oren, R., Takahashi, S., Doss, C., Levy, R. & Levy, S. TAPA-1, the target of an antiproliferative antibody, defines a new family of transmembrane proteins. *Mol. Cell. Biol.* **10**, 4007–4015 (1990).
25. D T Fearon & Carter, and R. H. The CD19/CR2/TAPA-1 Complex of B Lymphocytes: Linking Natural to Acquired Immunity. *Annu. Rev. Immunol.* **13**, 127–149 (1995).
26. Dornier, E. *et al.* TspanC8 tetraspanins regulate ADAM10/Kuzbanian trafficking and promote Notch activation in flies and mammals. *J. Cell Biol.* **199**, 481–496 (2012).
27. Nishiuchi, R. *et al.* Potentiation of the ligand-binding activity of integrin α3β1 via association with tetraspanin CD151. *Proc. Natl. Acad. Sci. U. S. A.* **102**, 1939–1944 (2005).
28. Liu, L. *et al.* Tetraspanin CD151 Promotes Cell Migration by Regulating Integrin Trafficking. *J. Biol. Chem.* **282**, 31631–31642 (2007).
29. Poulter, J. A. *et al.* Mutations in TSPAN12 Cause Autosomal-Dominant Familial Exudative Vitreoretinopathy. *Am. J. Hum. Genet.* **86**, 248–253 (2010).
30. Poulter, J. A. *et al.* Recessive Mutations in TSPAN12 Cause Retinal Dysplasia and Severe Familial Exudative Vitreoretinopathy (FEVR). *Invest. Ophthalmol. Vis. Sci.* **53**, 2873–2879 (2012).
31. Yang, H., Xiao, X., Li, S., Mai, G. & Zhang, Q. Novel TSPAN12 mutations in patients with familial exudative vitreoretinopathy and their associated phenotypes. *Mol. Vis.* **17**, 1128–1135 (2011).
32. Ju, Y. *et al.* Mutations in TSPAN12 gene causing familial exudative vitreoretinopathy. *Hum. Genomics* **18**, 22 (2024).
33. Kondo, H. *et al.* Mutations in the *TSPAN12* Gene in Japanese Patients with Familial Exudative Vitreoretinopathy. *Am. J. Ophthalmol.* **151**, 1095-1100.e1 (2011).
34. Lai, M. B. *et al.* TSPAN12 Is a Norrin Co-receptor that Amplifies Frizzled4 Ligand Selectivity and Signaling. *Cell Rep.* **19**, 2809–2822 (2017).
35. Junge, H. J. *et al.* TSPAN12 Regulates Retinal Vascular Development by Promoting Norrin- but Not Wnt-Induced FZD4/β-Catenin Signaling. *Cell* **139**, 299–311 (2009).
36. Knoblich, K. *et al.* Tetraspanin TSPAN12 regulates tumor growth and metastasis and inhibits β-catenin degradation. *Cell. Mol. Life Sci.* **71**, 1305–1314 (2014).
37. Bruguera, E. S., Mahoney, J. P. & Weis, W. I. The co-receptor Tetraspanin12 directly captures Norrin to promote ligand-specific β-catenin signaling. *eLife* **13**, RP96743 (2025).
38. Susa, K. J., Rawson, S., Kruse, A. C. & Blacklow, S. C. Cryo-EM structure of the B cell co-receptor CD19 bound to the tetraspanin CD81. *Science* **371**, 300–305 (2021).
39. Skiba, M. A. *et al.* Antibodies expand the scope of angiotensin receptor pharmacology. *Nat. Chem. Biol.* **20**, 1577–1585 (2024).
40. Tsutsumi, N. *et al.* Structure of human Frizzled5 by fiducial-assisted cryo-EM supports a heterodimeric mechanism of canonical Wnt signaling. *eLife* **9**, e58464 (2020).
41. Jumper, J. *et al.* Highly accurate protein structure prediction with AlphaFold. *Nature* **596**, 583–589 (2021).
42. Xiang, J. *et al.* Successful Strategies to Determine High-Resolution Structures of GPCRs. *Trends Pharmacol. Sci.* **37**, 1055–1069 (2016).
43. Mukherjee, S. *et al.* Synthetic antibodies against BRIL as universal fiducial marks for single−particle cryoEM structure determination of membrane proteins. *Nat. Commun.* **11**, 1598 (2020).
44. Ereño-Orbea, J. *et al.* Structural Basis of Enhanced Crystallizability Induced by a Molecular Chaperone for Antibody Antigen-Binding Fragments. *J. Mol. Biol.* **430**, 322–336 (2018).

45. Abramson, J. *et al.* Accurate structure prediction of biomolecular interactions with AlphaFold 3. *Nature* **630**, 493–500 (2024).
46. Zhang, X., Dong, S. & Xu, F. Structural and Druggability Landscape of Frizzled G Protein-Coupled Receptors. *Trends Biochem. Sci.* **43**, 1033–1046 (2018).
47. Yang, S. *et al.* Crystal structure of the Frizzled 4 receptor in a ligand-free state. *Nature* **560**, 666–670 (2018).
48. Qian, Y. *et al.* Structural basis of Frizzled 4 in recognition of Dishevelled 2 unveils mechanism of WNT signaling activation. *Nat. Commun.* **15**, 7644 (2024).
49. Hsieh, F.-L. & Chang, T.-H. Antibody Display of cell surface receptor Tetraspanin12 and SARS-CoV-2 spike protein. 2021.05.29.446300 Preprint at https://doi.org/10.1101/2021.05.29.446300 (2021).
50. Lipper, C. H., Egan, E. D., Gabriel, K.-H. & Blacklow, S. C. Structural basis for membrane-proximal proteolysis of substrates by ADAM10. *Cell* S009286742300733X (2023) doi:10.1016/j.cell.2023.06.026.
51. Bang, I. *et al.* Biophysical and functional characterization of Norrin signaling through Frizzled4. *Proc. Natl. Acad. Sci.* **115**, 8787–8792 (2018).
52. Berditchevski, F. & Odintsova, E. Tetraspanins as Regulators of Protein Trafficking. *Traffic* **8**, 89–96 (2007).
53. Shoham, T. *et al.* The Tetraspanin CD81 Regulates the Expression of CD19 During B Cell Development in a Postendoplasmic Reticulum Compartment. *J. Immunol.* **171**, 4062–4072 (2003).
54. Landau, M. *et al.* ConSurf 2005: the projection of evolutionary conservation scores of residues on protein structures. *Nucleic Acids Res.* **33**, W299–W302 (2005).
55. Zimmerman, B. *et al.* Crystal Structure of a Full-Length Human Tetraspanin Reveals a Cholesterol-Binding Pocket. *Cell* **167**, 1041-1051.e11 (2016).
56. Susa, K. J., Seegar, T. C., Blacklow, S. C. & Kruse, A. C. A dynamic interaction between CD19 and the tetraspanin CD81 controls B cell co-receptor trafficking. *eLife* **9**, e52337 (2020).
57. Umeda, R. *et al.* Structural insights into tetraspanin CD9 function. *Nat. Commun.* **11**, 1–11 (2020).
58. El Mazouni, D. & Gros, P. Cryo-EM structures of peripherin-2 and ROM1 suggest multiple roles in photoreceptor membrane morphogenesis. *Sci. Adv.* **8**, eadd3677 (2022).
59. Ke, J. *et al.* Structure and function of Norrin in assembly and activation of a Frizzled 4–Lrp5/6 complex. *Genes Dev.* **27**, 2305–2319 (2013).
60. Bowin, C.-F. *et al.* WNT stimulation induces dynamic conformational changes in the Frizzled-Dishevelled interaction. *Sci. Signal.* **16**, eabo4974 (2023).
61. Stoddart, L. A. *et al.* Application of BRET to monitor ligand binding to GPCRs. *Nat. Methods* **12**, 661–663 (2015).
62. Zhang, C. *et al.* Norrin-induced Frizzled4 endocytosis and endo-lysosomal trafficking control retinal angiogenesis and barrier function. *Nat. Commun.* **8**, 16050 (2017).
63. Chang, T.-H. *et al.* Structure and functional properties of Norrin mimic Wnt for signalling with Frizzled4, Lrp5/6, and proteoglycan. *eLife* **4**, e06554 (2015).
64. Shen, G. *et al.* Structural basis of the Norrin-Frizzled 4 interaction. *Cell Res.* **25**, 1078–1081 (2015).
65. Hirai, H., Matoba, K., Mihara, E., Arimori, T. & Takagi, J. Crystal structure of a mammalian Wnt–frizzled complex. *Nat. Struct. Mol. Biol.* **26**, 372–379 (2019).
66. Termini, C. M. & Gillette, J. M. Tetraspanins Function as Regulators of Cellular Signaling. *Front. Cell Dev. Biol.* **5**, (2017).
67. Zuidscherwoude, M. *et al.* Tetraspanin microdomains control localized protein kinase C signaling in B cells. *Sci. Signal.* **10**, eaag2755 (2017).

68. Logan, C. Y. & Nusse, R. THE WNT SIGNALING PATHWAY IN DEVELOPMENT AND DISEASE. *Annu. Rev. Cell Dev. Biol.* **20**, 781–810 (2004).
69. Bucher, F. *et al.* Antibody-Mediated Inhibition of Tspan12 Ameliorates Vasoproliferative Retinopathy Through Suppression of β-Catenin Signaling. *Circulation* **136**, 180–195 (2017).
70. Eubelen, M. *et al.* A molecular mechanism for Wnt ligand-specific signaling. *Science* **361**, eaat1178 (2018).
71. Bailey, L. J. *et al.* Locking the Elbow: Improved Antibody Fab Fragments as Chaperones for Structure Determination. *J. Mol. Biol.* **430**, 337–347 (2018).
72. Mastronarde, D. N. Automated electron microscope tomography using robust prediction of specimen movements. *J. Struct. Biol.* **152**, 36–51 (2005).
73. Punjani, A., Rubinstein, J. L., Fleet, D. J. & Brubaker, M. A. cryoSPARC: algorithms for rapid unsupervised cryo-EM structure determination. *Nat. Methods* **14**, 290–296 (2017).
74. Punjani, A., Zhang, H. & Fleet, D. J. Non-uniform refinement: adaptive regularization improves single-particle cryo-EM reconstruction. *Nat. Methods* **17**, 1214–1221 (2020).
75. Terwilliger, T. C., Ludtke, S. J., Read, R. J., Adams, P. D. & Afonine, P. V. *Improvement of Cryo-EM Maps by Density Modification*. http://biorxiv.org/lookup/doi/10.1101/845032 (2019) doi:10.1101/845032.
76. Sanchez-Garcia, R. *et al.* DeepEMhancer: a deep learning solution for cryo-EM volume post-processing. *Commun. Biol.* **4**, 874 (2021).
77. Emsley, P., Lohkamp, B., Scott, W. G. & Cowtan, K. Features and development of Coot. *Acta Crystallogr. D Biol. Crystallogr.* **66**, 486–501 (2010).
78. Pettersen, E. F. *et al.* UCSF ChimeraX: Structure visualization for researchers, educators, and developers. *Protein Sci. Publ. Protein Soc.* **30**, 70–82 (2021).
79. Adams, P. D. *et al.* PHENIX: a comprehensive Python-based system for macromolecular structure solution. *Acta Crystallogr. D Biol. Crystallogr.* **66**, 213–221 (2010).
80. Afonine, P. V. *et al.* Real-space refinement in PHENIX for cryo-EM and crystallography. *Acta Crystallogr. Sect. Struct. Biol.* **74**, 531–544 (2018).
81. Williams, C. J. *et al.* MolProbity: More and better reference data for improved all-atom structure validation. *Protein Sci. Publ. Protein Soc.* **27**, 293–315 (2018).
82. Barad, B. A. *et al.* EMRinger: side chain-directed model and map validation for 3D cryo-electron microscopy. *Nat. Methods* **12**, 943–946 (2015).
83. Morin, A. *et al.* Collaboration gets the most out of software. *eLife* **2**, e01456 (2013).